Molecular Vision 2019; 25:462-476 <http://www.molvis.org/molvis/v25/462>
Received 14 July 2019 | Accepted 19 August 2019 | Published 21 August 2019

Wheel running exercise protects against retinal degeneration in the I307N rhodopsin mouse model of inducible autosomal dominant retinitis pigmentosa

Xian Zhang,[1,2] Preston E. Girardot,[1] Jana T. Sellers,[1] Ying Li,[1] Jiaxing Wang,[1] Micah A. Chrenek,[1] Wenfei Wu,[1,3] Henry Skelton,[4] John M. Nickerson,[1] Machelle T. Pardue,[1,5,6] Jeffrey H. Boatright[1,5]

[1]Department of Ophthalmology, School of Medicine, Emory University, Atlanta, GA; [2]Department of Ophthalmology, Second Xiangya Hospital of Central South University, Changsha, Hunan, China; [3]The First Affiliated Hospital of Medical School of Xi'an Jiaotong University, Xi'an, Shan'xi, China; [4]Morehouse School of Medicine, Atlanta, GA; [5]Center for Visual and Neurocognitive Rehabilitation, Atlanta Veterans Administration Health Care System, Decatur, GA; [6]Department of Biomedical Engineering, Georgia Institute of Technology, Atlanta, GA

Purpose: We previously reported that modest running exercise protects photoreceptors in mice undergoing light-induced retinal degeneration and in the rd10 mouse model of autosomal recessive retinitis pigmentosa (arRP). We hypothesized that exercise would protect against other types of retinal degeneration, specifically, in autosomal dominant inherited disease. We tested whether voluntary running wheel exercise is protective in a retinal degeneration mouse model of class B1 autosomal dominant RP (adRP).

Methods: C57BL/6J mice heterozygous for the mutation in I307N rhodopsin (*Rho*) (also known as RHO$^{Tvrm4/+}$, or Tvrm4) are normal until exposed to brief but bright light, whereupon rod photoreceptor degeneration ensues. I307N *Rho* mice were given access to free spinning (active) or locked (inactive) running wheels. Five weeks later, half of each cohort was treated with 0.2% atropine eye drops and exposed to white LED light (6,000 lux) for 5 min, then returned to maintenance housing with wheels. At 1 week or 4 weeks after induction, retinal and visual function was assessed with electroretinogram (ERG) and optomotor response (OMR). In vivo retinal morphology was assessed with optical coherence tomography (OCT), and fundus blue autofluorescence assessed using a scanning laser ophthalmoscope. The mice were then euthanized, and the eyes fixed for paraffin sectioning or flatmounting. The paraffin sections were stained with hematoxylin and eosin (H&E) and terminal deoxynucleotidyl transferase dUTP nick-end labeling (TUNEL) to assess retina morphology and apoptosis. Half of the flatmounts were stained for ZO-1 and α-catenin to assess RPE cell structure and stress. (We previously reported that translocation of α-catenin from cell membranes into the cytosol indicates RPE cell stress.) The remaining flatmounts were stained for ZO-1 and Iba-1 to assess the RPE cell size and shape, and inflammatory responses.

Results: In vivo measures revealed that induction of the I307N *Rho* degeneration decreased retinal and visual function, decreased the thickness of the retina and photoreceptor layers, and increased the number of blue autofluorescence spots at the level of the photoreceptor–RPE interface. Post-mortem analyses showed that induction caused loss of photoreceptors in the central retinal region, and increased TUNEL labeling in the outer nuclear layer (ONL). The RPE was disrupted 1 week after induction, with changes in cell size and shape accompanied by increased α-catenin translocation and Iba-1 staining. These outcomes were partially but statistically significantly prevented in the exercised mice. The exercised mice that underwent induced I307N *Rho* degeneration exhibited retinal function and visual function measures that were statistically indistinguishable from that of the uninduced mice, and compared to the unexercised induced mice, had thicker retina and photoreceptor layers, and decreased numbers of subretinal autofluorescent spots. Post-mortem, the retina sections from the exercised mice that had undergone induced I307N *Rho* degeneration exhibited numbers of photoreceptors that were statistically indistinguishable from those of uninduced mice. Similarly, exercise largely precluded a degeneration-induced increase in TUNEL-positive cells in the ONL. Finally, the RPE of the exercised mice appeared normal, with a regular cell shape and size, and little to no alpha-catenin translocation or Iba-1 immunosignal.

Conclusions: Voluntary wheel running partially protected against retinal degeneration and inflammation, and RPE disruption in a model of inducible adRP. This is the first report of exercise protection in an adult adRP animal model. It is also the first report of an RPE phenotype in the I307N *Rho* mouse. These findings add to a growing literature reporting that modest whole-body exercise is protective across a wide range of models of retinal damage and disease, and further highlights the potential for this accessible and inexpensive therapeutic intervention in the ophthalmic clinic.

Correspondence to: Jeffrey H. Boatright, Department of Ophthalmology, Emory University, B5500, Clinic B Building,1365B Clifton Road, NE, Atlanta, GA 30322; Phone: (404)-778-4113; FAX: (404)-778-2231; email: jboatri@emory.edu

Retinitis pigmentosa (RP) is a group of retinal dystrophies affecting about 1.5 million people globally [1-3]. Mutations in more than 80 genes and loci have been linked to RP

(RetNet; July 1, 2019 update) [3-5]. Therapeutic strategies targeting specific mutations are being pursued [2,6-8], but with such a plethora of targets, it is arguably more efficient, and may have greater impact, to develop treatments that span genotypes. To that end, we tested and reported that treadmill running or voluntary wheel running is protective in a rat model of diabetic retinopathy [9], in mouse models of light-induced retinal degeneration (LIRD) [10-12], and in the rd10 mouse [13], a model of autosomal recessive RP (arRP) [14,15].

We sought to extend the translational relevance of our exercise intervention studies by testing in the I307N rhodopsin (*Rho*; also known as $RHO^{tvrm4/+}$) mouse model of autosomal dominant RP (adRP) [16-18]. This model is considered distinctly suitable for preclinical efficacy studies of potential RP therapies for several reasons [18]. First, mutations in RHO (Gene ID: 6010, OMIM 180380) account for a plurality of RP [3], and the I307N *Rho* mouse specifically mimics several aspects of the class B1 adRP phenotype [16-18]. Second, because the phenotype arises from chemical mutagenesis [16], it avoids the potential confound present for transgenic RP models that express mutant *Rho* in addition to wild-type [19], because overexpression of *Rho* alone can cause retinal degeneration [20]. Third, the degeneration is induced only upon brief exposure to bright light [16-18], allowing coordinated degeneration across all experimental subjects. Fourth, inducing in adolescence or later more closely mimics RP than commonly used models, such as rd1 or rd10 mouse models, that have degeneration onset in infancy, avoiding the potential developmental confounds of those models [14,15,18,21-23].

We report that voluntary wheel running statistically significantly preserved retinal function and morphology in induced I307 *Rho* mice. Additionally, we report for the first time that the I307N *Rho* degeneration includes RPE damage. This, too, was protected against in the wheel running cohorts.

METHODS

Animals: All mouse handling procedures and care were approved by the Emory Institutional Animal Care and Use Committee, and followed the ARVO Statement for the Use of Animals in Ophthalmic and Vision Research. A colony of I307N *Rho* mice was established and maintained at Emory by breeding homozygous I307N *Rho* mice (gift of Dr. Patsy Nishina of the Jackson Laboratory, Bar Harbor, ME; now available as catalog number 030,638) with C57BL/6J mice (Jackson Laboratories, catalog number 000,664) to produce heterozygous progeny for use in experiments [16,24]. (*N.B.*: The mice from Dr. Nishina originated from a two-generation backcross mating scheme using chemically mutated F1 hybrid 129/SvJae × C57BL/6J embryonic stem cells, followed by a minimum of five backcrosses onto the C57BL/6J background [16].) Mice were housed under a 12 h:12 h light-dark cycle (7 AM on and 7 PM off). During the light cycle, light levels measured at the bottom of the mouse cages ranged from 5 to 45 lux. Mice had access to standard mouse chow (Rodent Diet 5053; LabDiet, Inc., St. Louis, MO) ad libitum, and weighed 25 to 30 g throughout the study. Male and female mice aged 10–20 months were used in approximately equal numbers. Heterozygous I307N *Rho* mice were placed in single housing cages with low-profile running wheels (Med-Associates, Inc.; St. Albans, VT) that were either functional (active) or locked (inactive). All mice housed with active running wheels were observed twice daily to confirm running behavior. Mice had continuous access to wheels for the remainder of the experiment with the exception that, after 2 weeks of access, mice were temporarily moved to light chambers for induction of degeneration (detailed below), then transferred back to maintenance housing with active or inactive running wheels until the end of the experiment. Mice were euthanized by asphyxiation using CO_2 bottled gas for all experiments.

Induction of I307N Rho degeneration: Atropine eye drops (0.2% diluted from 1% atropine ophthalmic solution, Akorn Inc., Lake Forest, IL; diluted with Refresh Tears (Allergan, Irvine, TX)) were administered twice, with the last eye drops applied 30 min before toxic light exposure. For experimental light exposure to induce the I307N *Rho* degeneration, the animals were individually housed in white opaque polypropylene cages for 5 min without food or water while exposed to 6,000 lux levels of light from a white light-emitting diode light source. Exposure was between 10 and 11 AM (i.e., 3 to 4 h into the normal light cycle). After this exposure, the animals were returned to their home cages under normal lighting conditions for the remainder of the experiment. The uninduced mice were exposed to 50 lux light.

Electroretinograms: The complete electroretinogram (ERG) protocol was previously detailed [10,12,13,25,26]. Briefly, mice were dark-adapted overnight. In preparation for the ERGs, the mice were anesthetized with intraperitoneal (IP) injections of 100 mg/kg ketamine and 15 mg/kg xylazine (ketamine; KetaVed from Vedco, Saint Joseph, MO; xylazine.

Proparacaine (1%; Akorn Inc.) and tropicamide (1%; Akorn Inc.) eye drops were administered to reduce eye sensitivity and dilate the pupils. Once anesthetized, the mice were placed on a heating pad (39 °C) inside a Faraday cage in front of the desktop BigShot LED Ganzfeld stimulator (LKC Technologies, Gaithersburg, MD). A platinum wire fiber electrode, produced in-house, was placed in contact with each cornea. A drop of Refresh Tears (Allergan) was added to each eye to

maintain conductivity with the electrode fibers. The reference electrodes (LKC) were 1-cm needles inserted into each cheek, and the ground electrode (LKC) was placed in the tail. ERGs were recorded for the scotopic condition (0.00039–24.9000 cd s/m^2 and increasing flash stimulus intervals from 2.0 to 70 s). Mice recovered from anesthesia individually in cages placed partly on top of heated water pads.

In vivo ocular imaging: Spectral domain optical coherence tomography (SD-OCT) was conducted immediately after the ERG measurement, when the mice were still anesthetized, and their pupils were still dilated. A Micron IV SD-OCT system with fundus camera (Phoenix Research Labs, Pleasanton, CA) and a Heidelberg Spectralis HRA+OCT instrument with 25D lens (Heidelberg Engineering, Heidelberg, Germany) were used in tandem sequentially to assess ocular posterior segment morphology in section and en face. Using the Micron IV system, image-guided OCT images were obtained for the left and right eyes after a sharp and clear image of the fundus (with the optic nerve centered) was obtained. SD-OCT imaging was a circular scan about 100 µm from the optic nerve head. Fifty scans were averaged. The retinal layers were identified according to published nomenclature [27]. The total retinal thickness and thickness of the individual retinal layers were analyzed using Photoshop CS6 (Adobe Systems Inc., San Jose, CA). The number of pixels was converted into micrometers by multiplying by the micrometers per pixel conversion factor (1.3 µm = 1 pixel). Immediately after imaging on the Micron IV system, a rigid contact lens was placed on the eye (BOZR: 1.7 mm, Diameter: 3.2 mm, PWR: Plano), and blue autofluorescence imaging at the layer of the photoreceptor–RPE interface was conducted using the Heidelberg Spectralis HRA+OCT instrument. During imaging and afterward during anesthesia recovery, the mice were kept on water-circulating heat pads to maintain their body temperature.

Optomotor response: Visual acuity as a function of the spatial frequency threshold was measured by a trained observer-operator inducing and recording visual, reflexive, tracking behavior of individual mice using a virtual optomotor system (OptoMotry; Cerebral Mechanics, Inc., Lethbridge, Canada) as previously described [13,28]. The observer-operator was masked to the cohort membership of the mice. Briefly, a mouse was placed on a platform inside a chamber with four walls comprised of computer monitors displaying vertical dark and white lines in motion. The perceived visual environment was that of being inside a revolving cylinder of vertical stripes. The mouse moved its head left or right (depending on the direction the lines were spinning) to visually follow the movement of the lines in a reflexive tracking motion [29,30]. The spatial frequency in cycles per degree (i.e., the thickness of the dark lines) was progressively narrowed in a staircase pattern by the observer-operator until the mouse no longer made detectable head-tracking movements. The highest spatial frequency threshold at which tracking motions were still present was recorded as the mouse's visual acuity capability. Optomotor response (OMR) assessments were conducted under photopic conditions and at 100% line contrast 1 week and 4 weeks following toxic light exposure [30,31].

Histology and morphometrics of ocular sections: Histologic and morphometric procedures followed standard techniques [26]. Eyes were dehydrated, embedded in paraffin, and sectioned through the sagittal plane on a microtome at 5 µm increments. Sections containing the optic nerve and the center of the cornea were selected for staining to ensure that consistent regions were examined between animals. The slides were deparaffinized across five Coplin jars with 100 ml of xylene for 2 min each, consecutively. Then the slides were rehydrated in a series of 100 ml ethanol solutions for 2 min each: 100%, 90%, 80%, 70%, 60%, and 50%. The slides were immersed in PBS (137 mM NaCl, 2.7 mM KCl, 9.5 mM Phosphate buffer. pH 7.35) for 5 min each. After rehydration, terminal deoxynucleotidyl transferase dUTP nick-end labeling (TUNEL) assay was performed on some sections according to the protocol for the DeadEnd Fluorometric TUNEL Kit (Promega, Fitchburg, WI). Stained sections were imaged using fluorescent microscopy, and TUNEL-positive cells in the outer-nuclear layer (ONL) were manually counted for each whole retina using Adobe Photoshop Creative Suite 6 [25]. Some sections were used for hematoxylin and eosin (H&E) staining. ONL nuclei were counted in a semiautomated fashion using QuPath (University of Edinburgh, Division of Pathology, Edinburgh, Scotland; https://qupath.github.io) to outline the regions of the nuclei, and then to identify and count them within 100-µm-wide segments spaced at 250, 750, and 1,250 µm from the optic nerve head in the dorsal and ventral directions.

RPE flatmount tissue processing: The flatmounts were prepared similarly to our published approach [32-34]. Briefly, the superior side of the eye was marked with a blue Sharpie pen. Globes were fixed in Z-Fix (Anatech Ltd, Battle Creek, MI) for 10 min, and then washed three times with Hank's Balanced Salt Solution (HSBB; Cat. # 14025092, Gibco by Life Technologies, Grand Island, NY). RPE flatmounts were prepared using a microdissection technique as follows. Extraocular tissue was removed. The center of the cornea was punctured using 3 mm scissors, and four cuts were made extending from the cornea toward the optic nerve. The iris

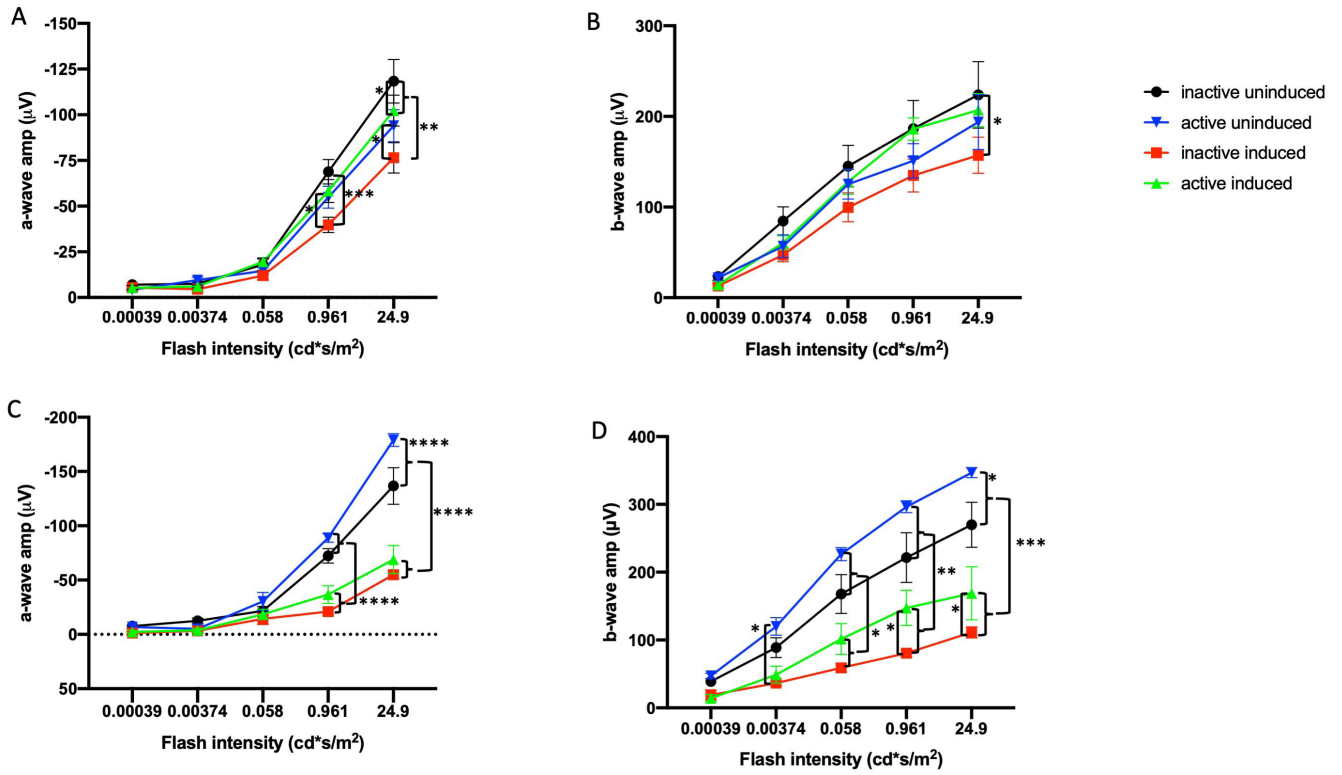

Figure 1. Exercise partially preserves retinal function in the I307N *Rho* mouse. Scotopic electroretinogram (ERG) a-wave (**A**, **C**) and b-wave (**B**, **D**) mean amplitudes from I307N *Rho* mice at 1 (**A**, **B**) and 4 weeks (**C**, **D**) after degeneration was induced. Mice with inactive running wheels and exposed to 6,000 lux light for 5 min to induce degeneration exhibited a- and b-wave mean amplitudes (red) that were statistically significantly diminished compared to those of the uninduced groups (blue and black). However, with the exception of the data in **C**, the mean ERG amplitudes of the mice undergoing retinal degeneration but with active running wheels (green) were either statistically indistinguishable from those of uninduced mice or were statistically significantly greater than those of the inactive induced mice. *p<0.05, **p<0.01, ***p<0.001, ****p<0.0001 with two-way ANOVA with the Newman-Keuls multiple comparisons test; comparisons as noted in the image. See Appendix 1, Appendix 2, Appendix 3, Appendix 4 for detailed tabular results and multiple comparisons. For each group in panels A–D, n=10–14 eyes. Error bars represent standard error of the mean (SEM).

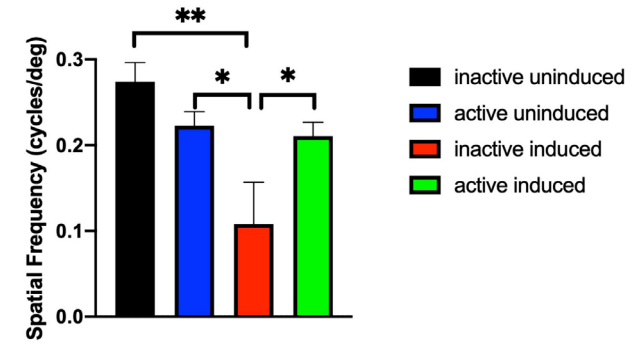

Figure 2. Exercise provides partial preservation of spatial frequency in induced I307N *Rho* degeneration mice. The inactive mice that underwent induced retinal degeneration (red bar) exhibited spatial frequency thresholds (as measured with optomotor response [OMR]) that were statistically significantly lower than those of the uninduced mice (black and blue bars) 4 weeks degeneration was induced. The induced mice that were active (green bar), however, exhibited a mean spatial frequency threshold that was statistically indistinguishable from those of the uninduced groups, but was statistically significantly greater than inactive, induced mice. **p<0.01 and *p<0.5 with one-way ANOVA with the Newman-Keuls multiple comparisons test; comparisons as indicated in figure. n=5–7 mice/group. Error bars represent standard error of the mean (SEM).

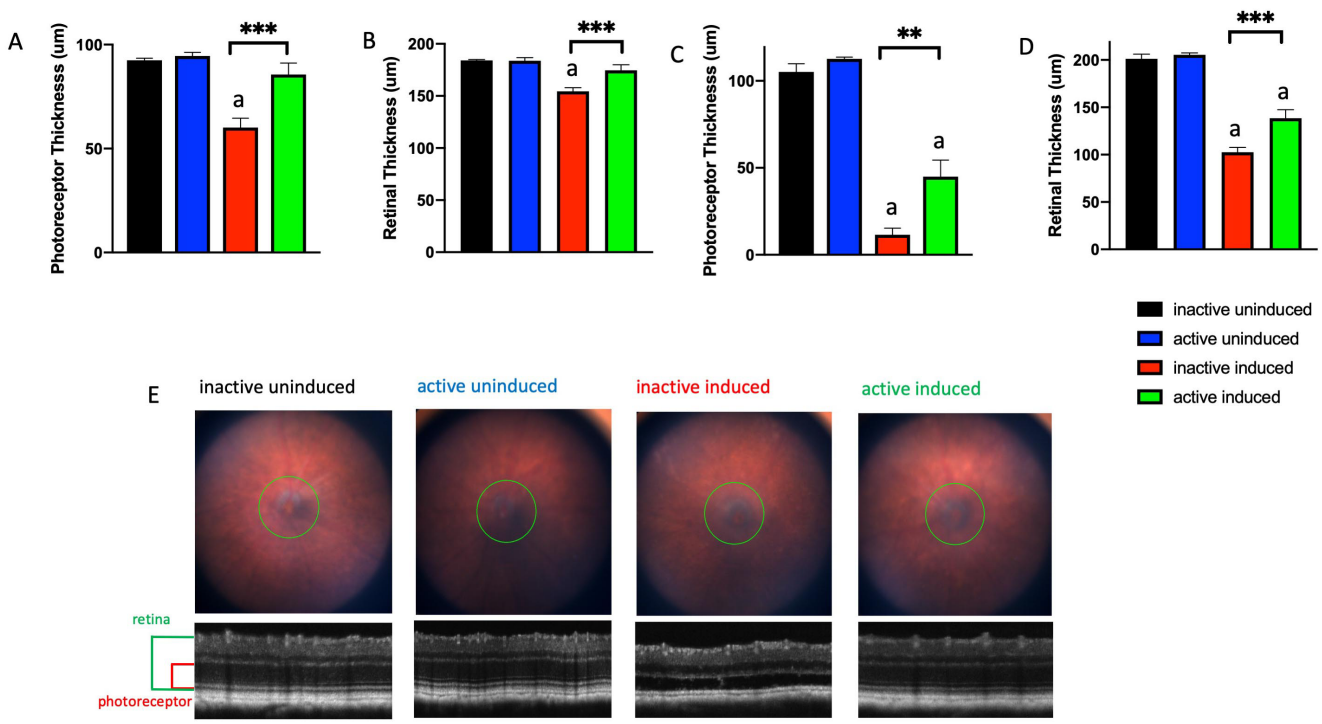

Figure 3. Exercise partially preserves photoreceptor layer thickness and total retinal thickness following induction of I307N *Rho* degeneration. Photoreceptor thickness (**A**, **C**) and retinal thickness (**B**, **D**) from I307N *Rho* mice at 1 (**A**, **B**) and 4 weeks (**C**, **D**) after degeneration was induced. The mice with inactive running wheels and exposed to 6,000 lux light for 5 min (red bar) exhibited losses in the thickness of the photoreceptor and retina layers, whereas the induced mice with active running wheels (green bar) exhibited statistically significant preservation of layer thickness. **E**. Representative fundus images and corresponding optical coherence tomography (OCT) images from each group. [a]p<0.05 versus all other groups. Other comparisons as indicated in the figure; **p<0.01, ***p<0.001 with one-way ANOVA with the Newman-Keuls multiple comparisons test. n=5–7 mice/group. Error bars represent standard error of the mean (SEM).

and the neural retina were removed. Four additional cuts were made in each of the four RPE-scleral flaps to enable the tissue to be flattened. After dissection, the tissues were flatmounted, RPE side up, on conventional microscope slides to which a silicon gasket had been applied (Grace Bio-Labs, Bend, OR). The flatmounts were rinsed with HBSS, followed by incubation with blocking buffer made with 1% bovine serum albumin (BSA; Sigma, St. Louis, MO) in 0.3% Triton X-100 (Sigma) HBSS solution 1 h at room temperature (RT).

Immunohistochemistry and confocal imaging of RPE flatmounts: The flatmounts were incubated with primary antibodies (1:250 anti-ZO-1, Cat. # MABT11, Sigma; 1:500 anti-CTAAN1, Cat. #EP1793Y, Abcam, Cambridge, MA; 1:1,000 anti-Iba-1, Cat. # 019–19741, Wako, Richmond, VA) overnight at RT. On the second day, the flatmounts were washed five times with 0.3% Triton X-100 in HBSS buffer, and then incubated with secondary antibodies (Alexa Fluor 488,1:1,000 donkey anti-rat immunoglobulin G (IgG), Cat. # A21208, Thermo Fisher Scientific, Waltham, MA; Alexa Fluor 568, 1:1,000 goat anti-rabbit IgG, Cat. # A11036, Thermo Fisher Scientific) overnight at RT. On the third day, the flatmounts were washed with Hoechst 33,258 (1:250, Cat. #H3569, Thermo Fisher Scientific) in blocking buffer three times, and then washed with HBSS in 0.3% Triton X-100 twice. Next, they were mounted with two drops of Fluoromount-G (Cat. #17984–25, Electron Microscopy Sciences, Signal Hill, CA), coverslipped, and allowed to set overnight. The slides were stored in the dark at 4 °C until imaging using a Nikon Ti inverted microscope with C1 confocal scanner (Nikon Instruments Inc., Melville, NY). Using an automated XY stage control within the EZ-C1 software, the flatmount was imaged with a 10X objective lens. Images were processed as described previously [33]. Briefly, confocal images from the entire flatmount were photomerged using Adobe Photoshop CS2, and zoning layers were applied.

Statistical analyses: One- and two-way repeated measures ANOVAs with post-hoc Newman-Keuls multiple comparisons test [35] and Student's *t* tests were performed for the ERG, OMR, and morphometric data. For all analyses, a p value of less than 0.05 was considered statistically significant.

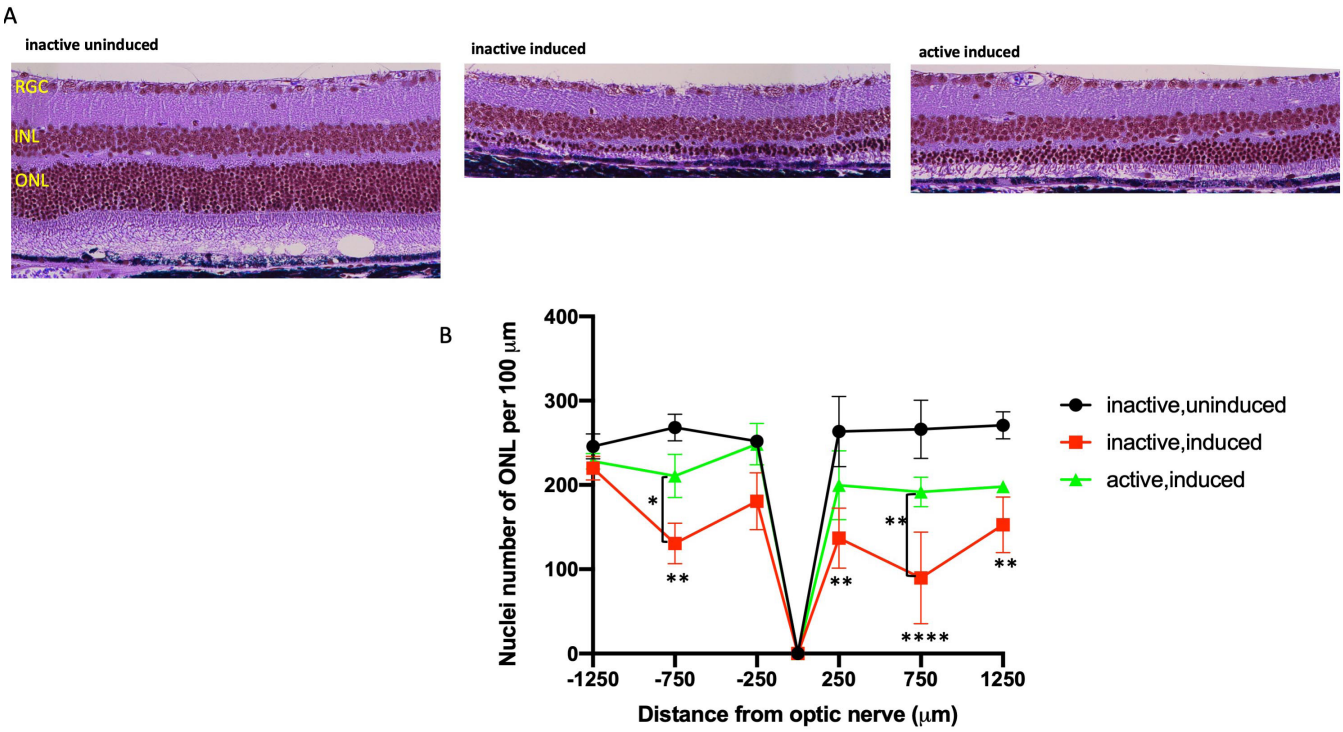

Figure 4. Exercise partially preserves outer nuclear layer in the I307N *Rho* retinal degeneration. I307N *Rho* degeneration was induced in active and inactive mice. A week later, the mice were euthanized, and ocular sections stained with hematoxylin and eosin (H&E). **A**: Representative H&E images of retina sections from each treatment group are from a region of 250–750 µm from the optic nerve. Examples of complete sections are shown in Appendix 5. **B**: Nuclei were counted in six discrete regions of the retinal sections starting at 250 µm from the optic nerve head and extending every 500 µm outward along the dorsal or superior (positive values on abscissa) and ventral periphery or inferior (negative numbers on abscissa); spacing and counting overlay templates are shown in Appendix 5. The inactive, induced mice (red) showed statistically significant loss of nuclei at four distances from the optic nerve head compared to the uninduced group (black); **p<0.01 and ****p<0.0001 versus the inactive, uninduced group. However, the induced mice that were active (green) exhibited mean nuclei counts statistically indistinguishable from those of the inactive, uninduced group (black) throughout the length of the retina. In the region of 250–750 µm superior and inferior from optic nerve, the nuclei counts were statistically greater in the active versus inactive induced mice; **p<0.01 and *p<0.05, comparisons as shown in the figure. All comparisons tested with two-way ANOVA with the Newman-Keuls multiple comparisons test. n=10–14 retinal images/group (five to seven mice/group). Error bars represent standard error of the mean (SEM).

All graphs display data as mean ± standard error of the mean (SEM). The stated n is the number of animals used in each group. Graphs and analyses were conducted using Prism 8.1.1 Software (GraphPad Software Inc., La Jolla, CA).

RESULTS

Exercise partially preserves retina and visual function in the I307N Rho mouse model of adRP: For mice housed with inactive running wheels, the I307N *Rho* degeneration resulted in significant diminution of ERG a- and b-wave mean amplitudes by 1 week following induction of degeneration compared to non-induced mice (Figure 1A,B; Appendix 1 and Appendix 2). This functional loss was partially prevented in induced mice with access to active running wheels, as their mean ERG amplitudes were not statistically significantly different from of those of the uninduced groups. In a replicate experiment, partial protection was obtained out to 4 weeks after degeneration was induced (Figure 1C,D; Appendix 3 and Appendix 4). Similarly, the I307N *Rho* degeneration resulted in about 40% diminution of the OMR spatial frequency threshold measured 4 weeks after induction ($p<0.05$). This functional loss was prevented in the induced mice with access to active running wheels: The spatial frequency of the exercised, induced mice was statistically indistinguishable from either group of uninduced mice, but was statistically significantly greater than that of the unexercised, induced mice (Figure 2). These data suggest that voluntary exercise protects photoreceptor and inner retina cell function and vision-directed behavior in this mouse model of adRP.

Exercise partially preserves retinal morphology in the I307N Rho mouse model of adRP: As imaged in vivo with SD-OCT 1 or 4 weeks after degeneration was induced, the

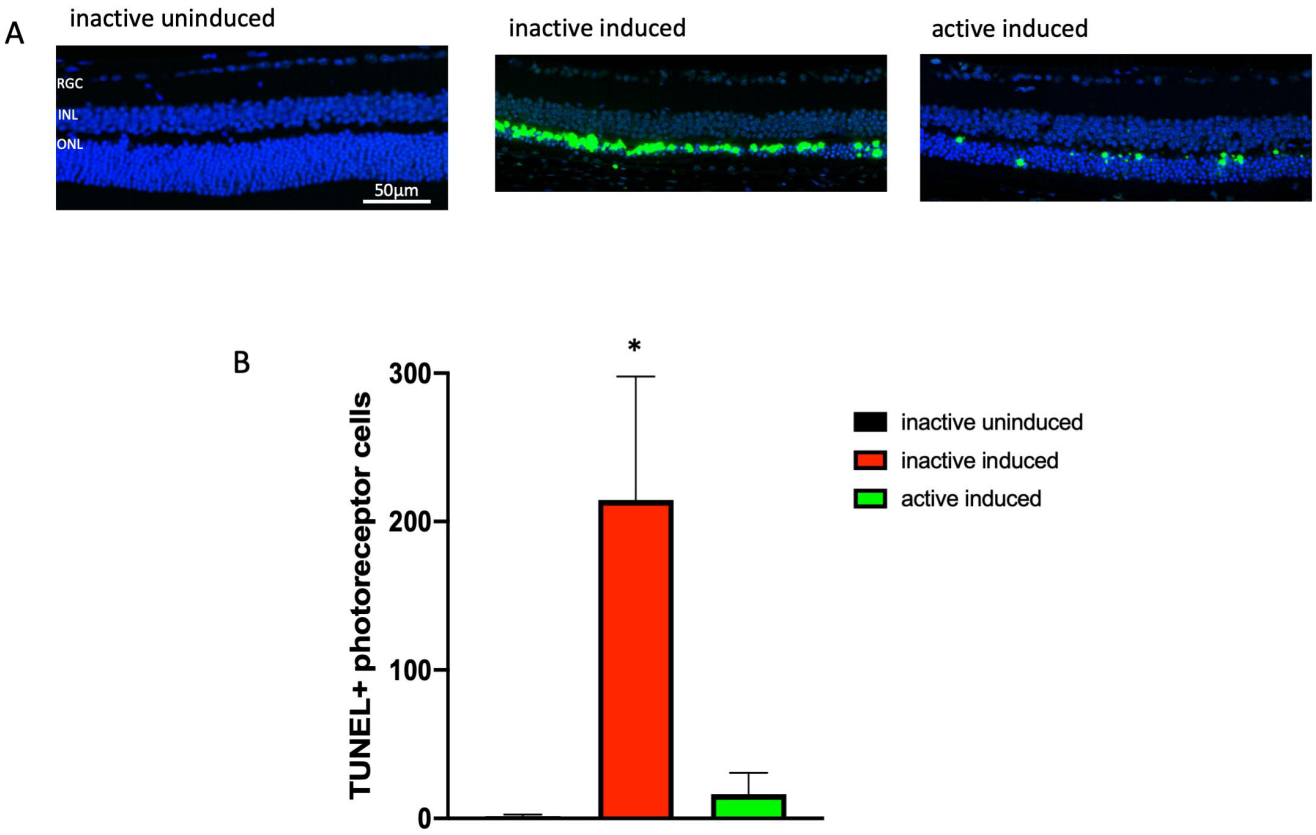

Figure 5. Exercise prevents increases in TUNEL-positive cells following induction of I307N Rho retinal degeneration. The active and inactive I307N *Rho* mice received toxic light exposure and were euthanized 1 week after exposure. Retinas were collected, sectioned, and sections were assayed for terminal deoxynucleotidyl transferase dUTP nick-end labeling (TUNEL). **A**: Representative morphological images of each group are from the region of 250–750 µm from the optic nerve. Complete sections are shown in Appendix 6. **B**: TUNEL-positive cells were counted across complete retina sections. The uninduced mice had few TUNEL-positive cells (black bar). Induction statistically significantly increased the number of TUNEL-positive cells per section (red bar). This increase did not occur in the active mice (green bar). *p<0.05 versus other groups with one-way ANOVA with the Newman-Keuls multiple comparisons test. n=3 sections/group. Error bars represent standard error of the mean (SEM). Size marker represents 50 µm.

retinas of I307N *Rho* mice housed with inactive running wheels thinned statistically significantly compared to those of the non-induced I307N *Rho* mice, largely due to thinning of the photoreceptor layer (Figure 3). Induced mice that ran on wheels showed statistically significantly less thinning of the retinas and photoreceptor layers as early as 1 week (Figure 3A,B), and as late as 4 weeks post-induction (Figure 3C,D). Representative fundus images and corresponding OCT images from each treatment group taken 1 week after degeneration was induced are shown in Figure 3E.

Photomicroscopy of H&E-stained sections of eyes harvested 1 week after induction showed marked degradation of morphology in the outer retina in the induced I307N *Rho* mice housed with inactive running wheels compared to those of the non-induced I307N *Rho* mice (Figure 4A,B and Appendix 5). Photoreceptor cell inner and outer segments and much of the nuclei of the ONL were eliminated, with the loss predominantly centrally (Figure 4A and Appendix 5) in induced mice housed with inactive running wheels. Conversely, much of this degeneration was prevented in the mice with active running wheels (Figure 4A and Appendix 5). Quantification of ONL nuclei counts confirmed statistically significant losses due to degeneration, and a lack of statistically significant loss in the exercised mice (Figure 4B). The morphological and morphometric data confirmed the I307N *Rho* phenotype previously reported [16-18], and indicated that voluntary wheel running is protective in this mouse model of adRP.

Exercise prevents accumulation of TUNEL signals in photoreceptor cells of induced I307N Rho mice: The

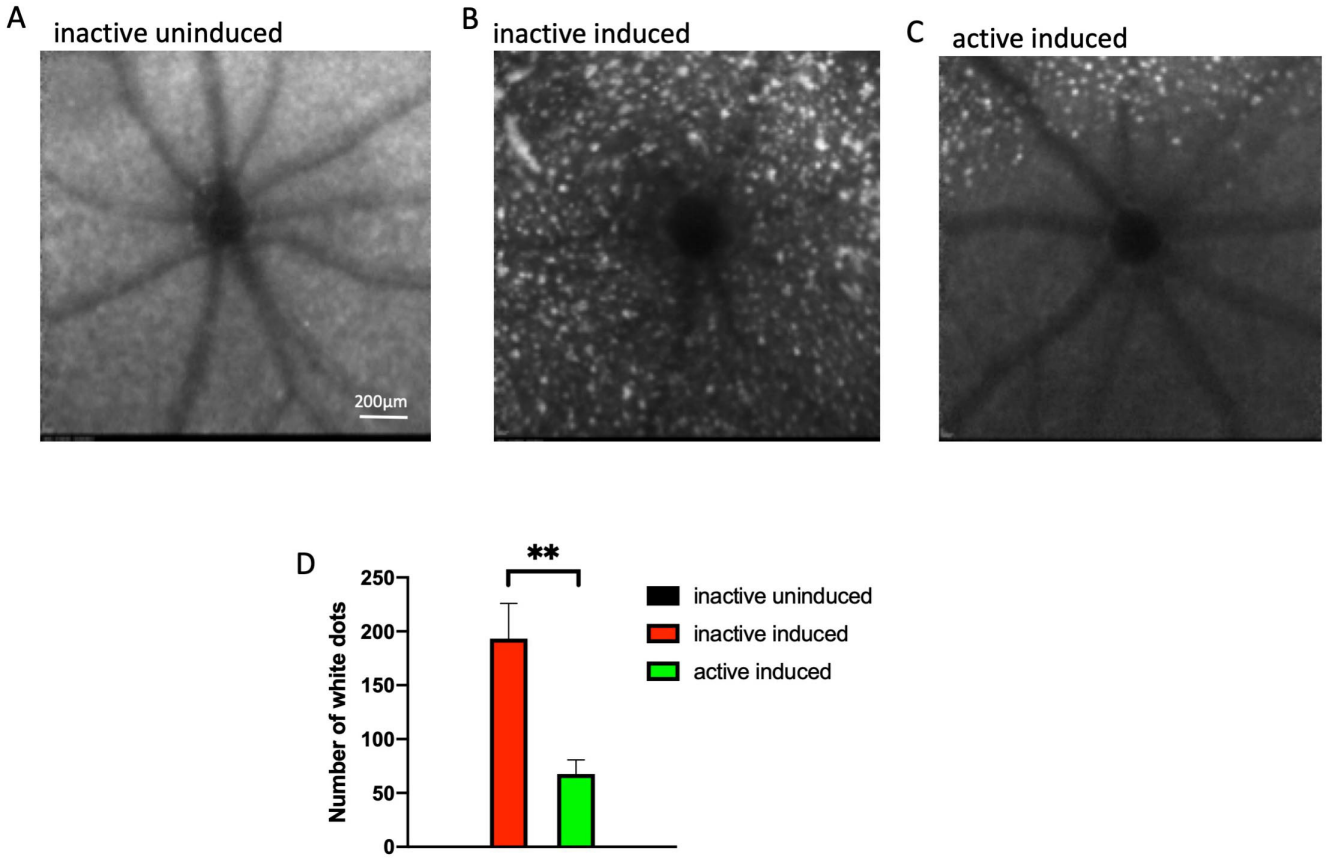

Figure 6. Exercise suppresses subretinal autofluorescence observed in the I307N *Rho* retinal degeneration. **A**–**C**: Representative morphology images from each group at the level of the photoreceptor–RPE interface. In vivo Spectralis HRA+OCT images (with blue autofluorescence detection) were taken 1 week after degeneration was induced. The top of each image is dorsal or superior, and the bottom is ventral periphery or inferior. In the mice induced to degenerate, autofluorescent white spots are numerous and widespread (**B** and **C**), though generally less dense in the inferior hemisphere in the exercised mice (**C**). **D**: Autofluorescent white spots were counted across the entire captured field of the fundus. None were detected in the uninduced mice. Active mice undergoing induced degeneration (green bar) exhibited statistically significantly fewer white spots compared to the inactive group (red bar). **p<0.005 by the Student *t* test. n=5–7 mice/group. Error bars are standard error of the mean (SEM). Size marker represents 200 µm.

paraffin-embedded ocular sections from the mice euthanized a week after induction were stained for TUNEL and 4′,6-diamidino-2-phenylindole (DAPI) to label nuclei with double-stranded DNA breaks (a hallmark of programmed cell death [apoptosis] or other forms of cell death). The ONL TUNEL signal was high in the retinas from the induced I307N *Rho* mice that had inactive running wheels compared to the retinas from the uninduced mice (Figure 5A and Appendix 6). The induced I307N *Rho* mice that ran on wheels exhibited statistically significantly less TUNEL signal (Figure 5B and Appendix 6). These data suggest that voluntary wheel running exercise diminished or delayed apoptosis in photoreceptor cells.

Exercise prevents an inflammatory response following induction of the I307N Rho retinal degeneration: Subretinal autofluorescent spots, dots, specks, or flecks observed in vivo with fundus examination are considered diagnostic markers for inflammatory responses in retinal damage and disease [36]. Similarly, the increased Iba-1 immunosignal in post-mortem RPE flatmounts is considered indicative of the presence of activated microglia and other inflammatory cells in models of retinal degeneration [37,38], including the I307N *Rho* mouse [17]. To test whether exercise alters inflammatory responses of the I307N phenotype, in vivo fundus examination at the level of the subretinal space was conducted 1 week following induction of I307N *Rho* degeneration, followed by euthanasia and harvest of the eyes for the subsequent fixation and immunohistochemical confocal microscopy on the RPE flatmounts. Uninduced eyes showed scant blue autofluorescence at the level of the subretinal space in vivo

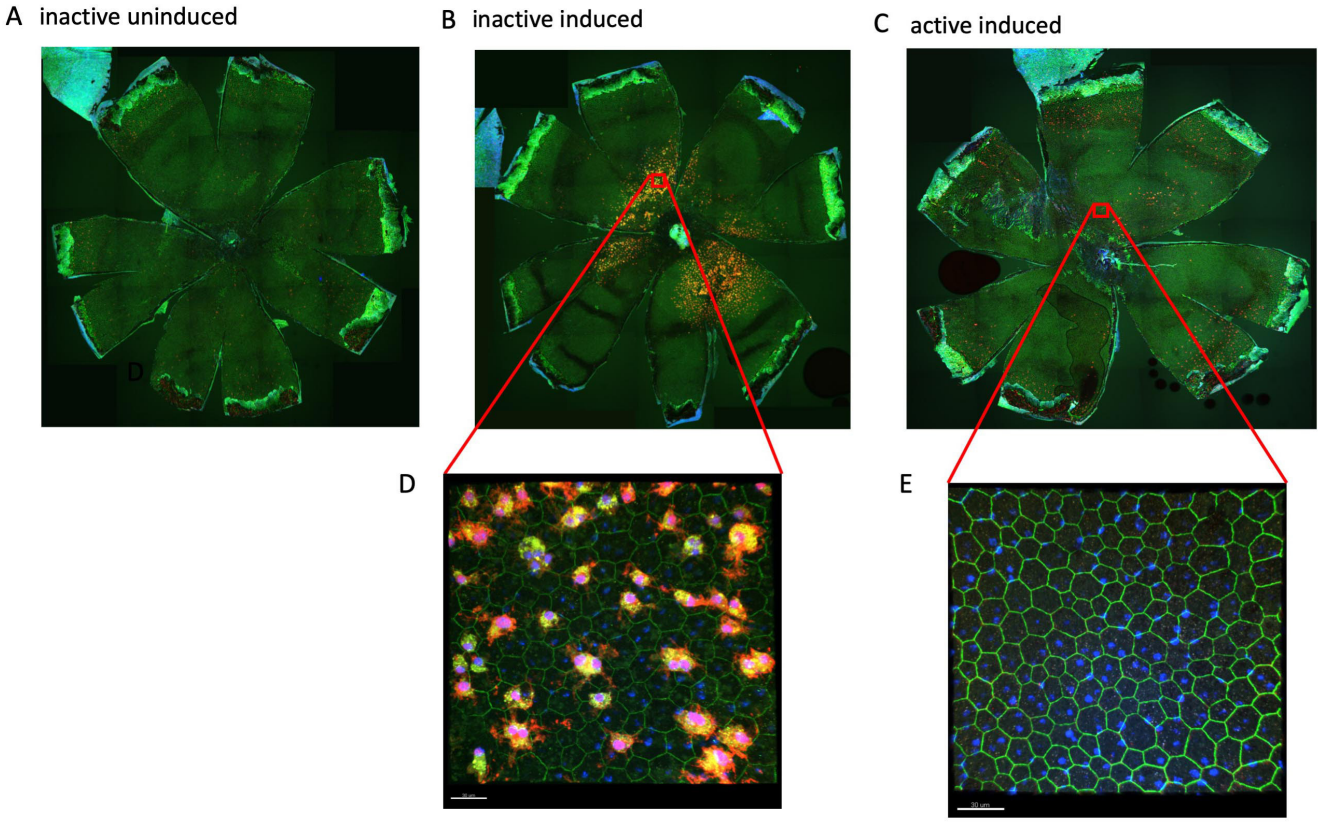

Figure 7. Exercise decreases an inflammatory response observed at the level of the RPE in I307N *Rho* retinal degeneration. The RPE flatmounts from the mice euthanized 1 week after degeneration was induced were immunostained for Iba-1 (red), ZO-1 (green), and 4′,6-diamidino-2-phenylindole (DAPI) (blue). **A**–**C**: Representative 100X fluorescent confocal microscopy images of flatmounts, RPE apical side facing up. **A**: Flatmounts from the uninduced, inactive mice had little or no Iba-1 immunosignal. **B**: Flatmounts from the inactive induced mice exhibited heavy Iba-1 staining. **C**: Flatmounts from the induced but active mice exhibited almost no Iba-1 staining, similar to samples from the uninduced mice. **D**: High-resolution image of the superior region from the inactive induced group; image taken at 600X magnification. **E**: High-resolution image of the superior region from the active induced group; image taken at 600X magnification. The size markers represent 30 µm.

(Figure 6A). In the eyes of the induced I307N *Rho* mice housed with inactive running wheels, numerous and widespread autofluorescent spots were observed in vivo (Figure 6B). This was prevented in the I307N *Rho* mice housed with active running wheels, which exhibited fewer autofluorescent spots in vivo (Figure 6C), confirmed with statistical testing of the counts of these spots (Figure 6D). The Iba-1 immunosignal in the post-mortem RPE flatmounts showed parallel outcomes. Flatmounts from uninduced mice showed few Iba-1-positive cells (Figure 7A), whereas numerous Iba-1-positive cells were observed in flatmounts from mice that had undergone degeneration (Figure 7B,D). This increase in Iba-1-positive cells was greatly diminished in the mice housed with active running wheels (Figure 7C,E). Additional examples of fundus autofluorescence images are paired with whole images of RPE flatmounts in Appendix 7. The overall patterns of the signal appear similar in the paired fundus and flatmount images. Finally, induction of degeneration statistically significantly increased the number of nucleated cellular infiltrates observed in the interphotoreceptor space (near the outer segment layers) of the inactive mice, but not that in the exercised mice (Appendix 5 and Figure 8). Similar infiltrates were seen in previous reports of the I307N *Rho* phenotype [16], but were not commented upon by the authors. The observations of autofluorescent spots, Iba-1 immunolabeled cells, and nucleated cellular infiltrates indicate that induction of the I307N *Rho* degeneration leads to an inflammatory response that is lessened by exercise, either indirectly (by partially preventing early rod photoreceptor injury) or more directly via as-yet undefined actions.

Exercise prevents RPE disruption: We previously reported that alpha-catenin, a member of the adherens junction protein complex that is required for maintaining the integrity of

epithelial cells [39], including RPE cells [40,41], translocates into the RPE cytosol following severe retinal degeneration [42], and that this may be an early event in the eventual RPE disruption. To assess whether the I307N *Rho* degeneration includes similar RPE disruption, the RPE flatmounts were stained with ZO-1 antibody to define the RPE cell borders, and with alpha-catenin antibody to locate alpha-catenin. The RPE of the uninduced I307N *Rho* mice had well-ordered RPE sheets with a high proportion of cells showing hexagonality (Figure 9A) and scant cytosolic alpha-catenin signal. Conversely, the RPE of the induced I307N *Rho* mice that had inactive running wheels was disrupted, with changes in size and shape, and high levels of alpha-catenin in the cytosol (Figure 9B,D). The RPE from the induced I307N *Rho* mice that had active running wheels looked similar to the RPE from the uninduced mice, with a high degree of ordered hexagonality and little or no cytosolic alpha-catenin signal (Figure 9C,E). Similar to our subretinal autofluorescence observation, these data indicate that exercise may prevent RPE disruption. This may be epiphenomenal, e.g., secondary to protection of photoreceptors, or it may be by undefined direct actions on the RPE.

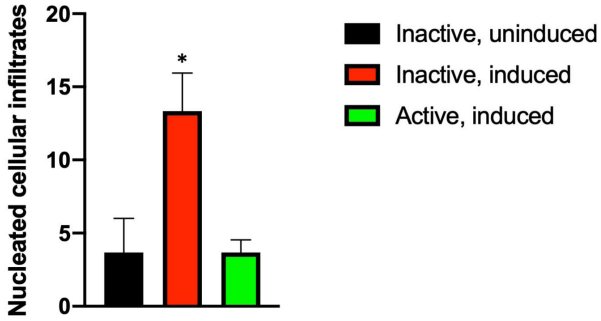

Figure 8. Exercise prevents accumulation of nucleated cellular infiltrates in the interphotoreceptor space. As observed in Figure 4 and Appendix 5, induction of I307N *Rho* degeneration increased the number of nucleated cellular infiltrates in the interphotoreceptor space (near the outer segment layer) of the inactive mice. Counting these infiltrates across entire retinal sections revealed that the induced, inactive mice (red bar) had statistically significantly more infiltrates compared to uninduced mice (black bar). However, this increase was prevented in exercised mice (green bar). *p<0.05 versus other groups with one-way ANOVA with the Newman-Keuls multiple comparisons test. n=3 sections/group. Error bars represent standard error of the mean (SEM).

DISCUSSION

Induction of I307N *Rho* retinal degeneration resulted in retinal and visual function deficits and degeneration of photoreceptor cells, corroborating outcomes well documented by three independent groups reporting characterizations of this adRP model [16-18]. We add to this characterization with the observations that the degeneration etiology includes the appearance of subretinal autofluorescent spots, evidence of rammified Iba-1-positive cells (presumptive activated microglia) observed at the apical surface of the RPE, and RPE disruption. Voluntary wheel running statistically significantly protected against these pathological processes, observed as better retinal and visual outcomes, suppressed inflammatory response, and preservation of RPE cell and sheet morphology. The functional and morphological protective effects are in agreement with similar outcomes from our exercise studies with other retinal disease or damage models [9-13] and those of others [43-46]. With the exception of our study [12] of the effects of voluntary wheel running on the rd10 mouse (an arRP model confounded by the degeneration occurring during development), these studies were conducted with forced exercise (e.g., swimming or treadmill running), which can induce stress [12], and thus, confound interpretation of results. Thus, we report protection with a clinically relevant exercise modality in a model of adRP that extends the potentially clinical significance of studies testing effects of exercise on models of ocular disease.

The RPE disruption we observed in the present study is suggested by changes in RPE cell size and shape, and alpha-catenin translocation from RPE cell membrane to the cytosol (Figure 9). Alpha-catenin is a mechanosensor that binds F-actin to couple the cadherin-catenin complex to the actin cytoskeleton at adherens junctions [47] that are required for maintaining the integrity of epithelial cells [39], including RPE cells [40]. Mutations in alpha-catenin lead to RPE abnormalities and butterfly pattern macular dystrophy [41]. Release of alpha-catenin into the cytosol thus may represent an early and significant event in RPE cell degradation [42]. That exercise protects against alpha-catenin translocation may be simply due to exercise partially preventing photoreceptor degeneration that would have eventually induced RPE disruption, or exercise may have direct effects on RPE physiology. Testing the potential causative paths requires additional study.

Although the specific I307N *Rho* mutation has not been reported in humans, and its associated retinal degeneration is rapid, rather than slow as in most presentations of RP, the I307N *Rho* mouse model is useful for preclinical studies [16-18]. It is significant translationally due to its autosomal dominant genetics, its clear pattern and time course of photoreceptor cell degeneration, and its ease of study with common clinical diagnostic approaches, e.g., ERG, fundus

examination, and SD-OCT [16-18]. The observation of autofluorescent spots with fundus examination adds to this potential translational significance in that such hyperautofluorescence is considered a useful in vivo diagnostic tool in the clinic [36].

Autofluorescent spots similar to those observed here are postulated to be components of inflammatory responses (e.g., activated microglial cells [48], lipofuscin in RPE cells, and bisretinoids in the photoreceptors [49-51], RPE cells undergoing epithelial-mesenchymal transition (EMT) that are migrating into the neural retina [52,53], etc.). The present data indicated that exercise prevents the appearance of these autofluorescing entities, and thus, may be preventing retinal inflammation, either indirectly by partially preventing early rod photoreceptor injury, or more directly by some as-yet undefined action. Comparing the patterns of autofluorescent spots in images in Figure 6 with the Iba-1-postive cells in images in Figure 7, it appears likely that at least some of these autofluorescent spots are microglia in the subretinal space (the plane of focus for the images of Figure 6 and Figure 7), possibly activated due to photoreceptor degeneration or RPE disruption. Similar Iba-1 immunostaining indicating activation of microglia and migration into the outer retina was thoroughly documented for the I307N *Rho* mouse by Strettoi and colleagues [17], while Swaroop and colleagues have suggested that autofluorescent spots in the subretinal space are subretinal accumulations of microglia activated by RPE atrophy [48]. Though speculative, the nucleated cellular

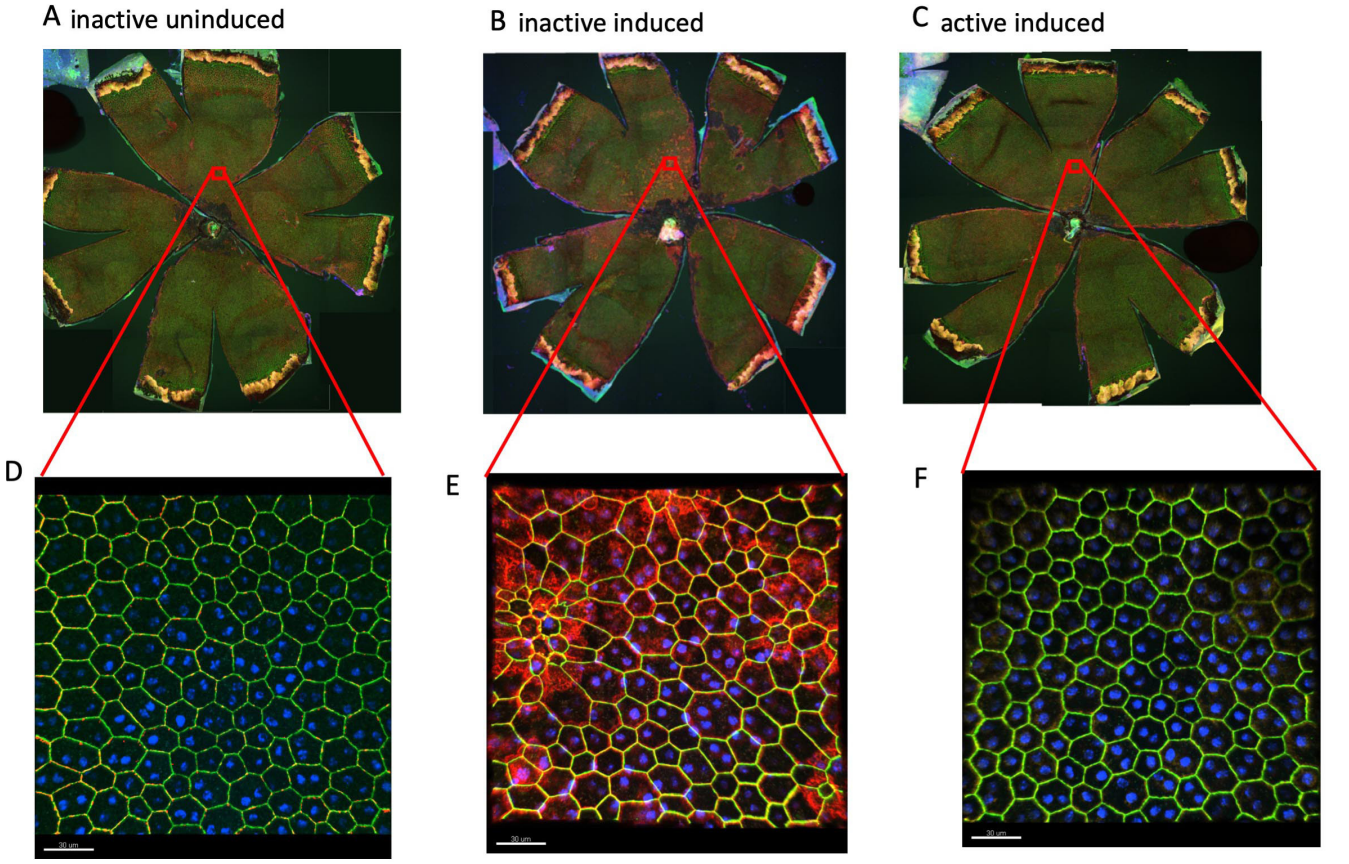

Figure 9. Exercise prevents RPE stress in I307N *Rho* retinal degeneration. RPE stress is suggested by alpha-catenin translocation from cell borders into cytosol [42]. RPE flatmounts (RPE apical side facing up) from the mice euthanized 1 week after degeneration was induced were immunostained for alpha-catenin (red), ZO-1 (green), and 4′,6-diamidino-2-phenylindole (DAPI) (blue). **A**–**C**: Representative 100X fluorescent confocal microscopy images of flatmounts. **D**–**F**: High-resolution images of the superior region from the inactive uninduced (**D**), inactive induced (**E**), or active induced group (**F**); images taken at 600X magnification. Flatmounts from the uninduced, inactive mice had little or no cytosolic alpha-catenin immunosignal (**A** and **D**). Flatmounts from the inactive induced mice exhibited heavy cytosolic alpha-catenin immunostaining, particularly in the regions of cells with distortion in shape and changes in size (**B** and **E**). Flatmounts from the induced but active mice exhibited almost no cytosolic alpha-catenin staining, similar to the samples from the uninduced mice, with nearly unperturbed RPE cell shape and size (**C** and **F**). The size markers represent 30 µm.

infiltrates observed in the interphotoreceptor space of mice undergoing I307N *Rho* retinal degeneration may be activated microglia or invading macrophages. If so, the finding that mice with active running wheels had significantly fewer infiltrates additionally suggests that exercise prevents or suppresses degeneration-induced retinal inflammation.

In summary, we present data that extend the potential translational relevance of studies testing the effects of whole-body exercise on retinal damage and disease. The I307N *Rho* model of adRP, though having aggressive retinal degeneration, responded well to a wheel-running exercise intervention, which is voluntary, and may more closely mimic human exercise compared to forced exercise in animal models. Evidence continues to accumulate suggesting that modest exercise may be an accessible and inexpensive intervention for retinal degenerative diseases.

APPENDIX 1.

Detailed tabular results and multiple comparisons from two-way ANOVA of ERG a-wave data from experiment testing effects of exercise on induced and uninduced I307N Rho mice one week following induction (graphically shown in Figure 1A). To access the data, click or select the words "Appendix 1."

APPENDIX 2.

Detailed tabular results and multiple comparisons from two-way ANOVA of ERG b-wave data from experiment testing effects of exercise on induced and uninduced I307N Rho mice one week following induction (graphically shown in Figure 1B). To access the data, click or select the words "Appendix 2."

APPENDIX 3.

Detailed tabular results and multiple comparisons from two-way ANOVA of ERG a-wave data from experiment testing effects of exercise on induced and uninduced I307N Rho mice four weeks following induction (graphically shown in Figure 1C). To access the data, click or select the words "Appendix 3."

APPENDIX 4.

Detailed tabular results and multiple comparisons from two-way ANOVA of ERG b-wave data from experiment testing effects of exercise on induced and uninduced I307N Rho mice four weeks following induction (graphically shown in Figure 1D).To access the data, click or select the words "Appendix 4."

APPENDIX 5.

Figure showing full-sized images that suggest that exercise partially preserves nuclei of the outer nuclear layer in the I307N *Rho* retinal degeneration. The I307N *Rho* degeneration was induced in active and inactive mice. A week later the mice were euthanized and ocular sections stained with hematoxylin and eosin (H&E). Representative H&E images of complete retina sections from each treatment group are shown with six spacing and counting overlay templates per section as used for quantification of nuclei of the outer nuclear layer starting at 250 µm from the optic nerve head and extending every 500 µm outward along both the dorsal/superior (right half of each section) and ventral periphery/inferior (left half of each section). The same set of high-resolution images of complete retina sections were used for quantification of nucleated cell infiltrates observed the interphotoreceptor space (quantification presented in Figure 8). Examples of nucleated infitrates are pointed to by arrows. **A**: Section from an inactive, uninduced mouse shows unperturbed ONL across the span of the retina. **B**: Section from an inactive, induced mouse shows extreme thinning in the central, superior (right side of section) ONL. **C**: Section from an active, induced mouse shows diminished thinning ONL relative to inactive mouse. To access the data, click or select the words "Appendix 5."

APPENDIX 6.

Figure showing full-sized images that suggest that exercise prevents accumulation of TUNEL signal in photoreceptor cells of induced I307N *Rho* mice. The I307N *Rho* degeneration was induced in active and inactive mice. A week later the mice were euthanized and ocular sections stained for TUNEL (green) and DAPI (blue). Representative images of complete retina sections from each treatment group are shown. The right half of each section is dorsal/superior and the left half is ventral periphery/inferior. **A**: Section from an inactive, uninduced mouse shows little to no TUNEL-positive ONL nuclei across the span of the retina. **B**: Section from an inactive, induced mouse shows numerous TUNEL-positive ONL nuclei in both superior and inferior halves. **C**: Section from an active, induced mouse shows almost no TUNEL-positive ONL nuclei in inferior half and diminished numbers of TUNEL-positive ONL nuclei relative to inactive mouse sections in the superior half. To access the data, click or select the words "Appendix 6."

APPENDIX 7.

Figure showing full-sized images that allow comparison of fundus autofluorescent spots observed in vivo with Iba-1 immuno-signal in post-mortem RPE flatmount from the same eye. In vivo fundus examination at the level of the subretinal space was conducted one week following induction of the I307N *Rho* degeneration, followed by euthanization and harvest of eyes for subsequent fixation and immunohistochemical confocal microscopy on RPE flatmounts. **A:** Uninduced eyes showed scant blue autofluorescence at the level of the subretinal space in vivo (left) and RPE flatmouns of those same eyes showed little Iba-1 immuno-signal (right). **B:** In eyes of induced I307N *Rho* mice housed with inactive running wheels, numerous and widespread autofluorescent spots were observed in vivo (left) and matching flatmounts exhibited numerous Iba-1-positive cells (right). **C:** Exercised mice that had undergone degeneration induction showed greatly diminished numbers of autofluorescent spots (left) and Iba-1-positive cells (right). Overall patterns of signal appear similar in paired fundus and flatmount images, suggesting the possibility that some autoflourescent spots observed via in vivo fundus imaging are likely to be overexpressing Iba-1 and may be microglia or other inflammatory cells. To access the data, click or select the words "Appendix 7."

ACKNOWLEDGMENTS

Abraham J and Phyllis Katz Foundation (JHB); The joint training program between Emory University School of Medicine and Xiangya School of Medicine, Central South University. China Scholarship Council (XZ); VA Research Career Scientist Award IK6 RX003134 (MTP); NIH R01EY028859 (JHB & MTP); NIH R01EY021592 (JMN); NIH R01EY028450 (JMN); VA I01RX002806 (JHB); VA I21RX001924 (JHB); VARR&D C9246C (Atlanta VAMC); NIH P30EY06360 (Emory); Research to Prevent Blindness (Emory).

REFERENCES

1. Verbakel SK, van Huet RAC, Boon CJF, den Hollander AI, Collin RWJ, Klaver CCW, Hoyng CB, Roepman R, Klevering BJ. Non-syndromic retinitis pigmentosa. Prog Retin Eye Res 2018; 66:157-86. [PMID: 29597005].
2. Zhang Q. Retinitis Pigmentosa: Progress and Perspective. Asia Pac J Ophthalmol (Phila) 2016; 5:265-71. [PMID: 27488069].
3. Jones KD, Wheaton DK, Bowne SJ, Sullivan LS, Birch DG, Chen R, Daiger SP. Next-generation sequencing to solve complex inherited retinal dystrophy: A case series of multiple genes contributing to disease in extended families. Mol Vis 2017; 23:470-81. [PMID: 28761320].
4. Daiger SP, Sullivan LS, Bowne SJ. RetNet The Retinal Information Network. July 1, 2019 ed: The Univ. of Texas Health Science Center at Houston; 2019
5. Rossmiller B, Mao H, Lewin AS. Gene therapy in animal models of autosomal dominant retinitis pigmentosa. Mol Vis 2012; 18:2479-96. [PMID: 23077406].
6. Bassuk AG, Zheng A, Li Y, Tsang SH, Mahajan VB. Precision Medicine: Genetic Repair of Retinitis Pigmentosa in Patient-Derived Stem Cells. Sci Rep 2016; 6:19969-[PMID: 26814166].
7. Zheng A, Li Y, Tsang SH. Personalized therapeutic strategies for patients with retinitis pigmentosa. Expert Opin Biol Ther 2015; 15:391-402. [PMID: 25613576].
8. Wiley LA, Burnight ER, Songstad AE, Drack AV, Mullins RF, Stone EM, Tucker BA. Patient-specific induced pluripotent stem cells (iPSCs) for the study and treatment of retinal degenerative diseases. Prog Retin Eye Res 2015; 44:15-35. [PMID: 25448922].
9. Allen RS, Hanif AM, Gogniat MA, Prall BC, Haider R, Aung MH, Prunty MC, Mees LM, Coulter MM, Motz CT, Boatright JH, Pardue MT. TrkB signalling pathway mediates the protective effects of exercise in the diabetic rat retina. Eur J Neurosci 2018; 47:1254-65. [PMID: 29537701].
10. Lawson EC, Han MK, Sellers JT, Chrenek MA, Hanif A, Gogniat MA, Boatright JH, Pardue MT. Aerobic exercise protects retinal function and structure from light-induced retinal degeneration. J Neurosci 2014; 34:2406-12. [PMID: 24523530].
11. Chrenek MA, Sellers JT, Lawson EC, Cunha PP, Johnson JL, Girardot PE, Kendall C, Han MK, Hanif A, Ciavatta VT, Gogniat MA, Nickerson JM, Pardue MT, Boatright JH. Exercise and Cyclic Light Preconditioning Protect Against Light-Induced Retinal Degeneration and Evoke Similar Gene Expression Patterns. Adv Exp Med Biol 2016; 854:443-8. [PMID: 26427444].
12. Mees LM, Coulter MM, Chrenek MA, Motz CT, Landis EG, Boatright JH, Pardue MT. Low-Intensity Exercise in Mice Is Sufficient to Protect Retinal Function During Light-Induced Retinal Degeneration. Invest Ophthalmol Vis Sci 2019; 60:1328-35. [PMID: 30933260].
13. Hanif AM, Lawson EC, Prunty M, Gogniat M, Aung MH, Chakraborty R, Boatright JH, Pardue MT. Neuroprotective Effects of Voluntary Exercise in an Inherited Retinal Degeneration Mouse Model. Invest Ophthalmol Vis Sci 2015; 56:6839-46. [PMID: 26567796].
14. Chang B, Hawes NL, Hurd RE, Davisson MT, Nusinowitz S, Heckenlively JR. Retinal degeneration mutants in the mouse. Vision Res 2002; 42:517-25. [PMID: 11853768].
15. Chang B, Hawes NL, Pardue MT, German AM, Hurd RE, Davisson MT, Nusinowitz S, Rengarajan K, Boyd AP, Sidney SS, Phillips MJ, Stewart RE, Chaudhury R, Nickerson JM, Heckenlively JR, Boatright JH. Two mouse retinal degenerations caused by missense mutations in the beta-subunit of rod cGMP phosphodiesterase gene. Vision Res 2007; 47:624-33. [PMID: 17267005].

16. Budzynski E, Gross AK, McAlear SD, Peachey NS, Shukla M, He F, Edwards M, Won J, Hicks WL, Wensel TG, Naggert JK, Nishina PM. Mutations of the opsin gene (Y102H and I307N) lead to light-induced degeneration of photoreceptors and constitutive activation of phototransduction in mice. J Biol Chem 2010; 285:14521-33. [PMID: 20207741].

17. Gargini C, Novelli E, Piano I, Biagioni M, Strettoi E. Pattern of retinal morphological and functional decay in a light-inducible, rhodopsin mutant mouse. Sci Rep 2017; 7:5730-[PMID: 28720880].

18. Massengill MT, Young B, Patel D, Jafri F, Sabogal E, Ash N, Li H, Ildefonso CJ, Lewin AS. Clinically Relevant Outcome Measures for the I307N Rhodopsin Mouse: A Model of Inducible Autosomal Dominant Retinitis Pigmentosa. Invest Ophthalmol Vis Sci 2018; 59:5417-30. [PMID: 30452595].

19. Olsson JE, Gordon JW, Pawlyk BS, Roof D, Hayes A, Molday RS, Mukai S, Cowley GS, Berson EL, Dryja TP. Transgenic mice with a rhodopsin mutation (Pro23His): a mouse model of autosomal dominant retinitis pigmentosa. Neuron 1992; 9:815-30. [PMID: 1418997].

20. Tan E, Wang Q, Quiambao AB, Xu X, Qtaishat NM, Peachey NS, Lem J, Fliesler SJ, Pepperberg DR, Naash MI, Al-Ubaidi MR. The relationship between opsin overexpression and photoreceptor degeneration. Invest Ophthalmol Vis Sci 2001; 42:589-600. [PMID: 11222515].

21. Dutta S, Sengupta P. Men and mice: Relating their ages. Life Sci 2016; 152:244-8. [PMID: 26596563].

22. Sidman RL, Green MC. Retinal Degeneration in the Mouse: Location of the Rd Locus in Linkage Group Xvii. J Hered 1965; 56:23-9. [PMID: 14276177].

23. Lolley RN. Changes in glucose and energy metabolism in Vivo in developing retinae from visually-competent (DBA-1J) and mutant (C3H-HeJ) mice. J Neurochem 1972; 19:175-85. [PMID: 5009894].

24. Won J, Shi LY, Hicks W, Wang J, Hurd R, Naggert JK, Chang B, Nishina PM. Mouse model resources for vision research. J Ophthalmol 2011; 2011:391384-[PMID: 21052544].

25. Boatright JH, Moring AG, McElroy C, Phillips MJ, Do VT, Chang B, Hawes NL, Boyd AP, Sidney SS, Stewart RE, Minear SC, Chaudhury R, Ciavatta VT, Rodrigues CM, Steer CJ, Nickerson JM, Pardue MT. Tool from ancient pharmacopoeia prevents vision loss. Mol Vis 2006; 12:1706-14. [PMID: 17213800].

26. Phillips MJ, Walker TA, Choi HY, Faulkner AE, Kim MK, Sidney SS, Boyd AP, Nickerson JM, Boatright JH, Pardue MT. Tauroursodeoxycholic acid preservation of photoreceptor structure and function in the rd10 mouse through postnatal day 30. Invest Ophthalmol Vis Sci 2008; 49:2148-55. [PMID: 18436848].

27. Huber G, Beck SC, Grimm C, Sahaboglu-Tekgoz A, Paquet-Durand F, Wenzel A, Humphries P, Redmond TM, Seeliger MW, Fischer MD. Spectral domain optical coherence tomography in mouse models of retinal degeneration. Invest Ophthalmol Vis Sci 2009; 50:5888-95. [PMID: 19661229].

28. Henneman NF, Foster SL, Chrenek MA, Sellers JT, Wright CB, Schmidt RH, Nickerson JM, Boatright JH. Xanthohumol Protects Morphology and Function in a Mouse Model of Retinal Degeneration. Invest Ophthalmol Vis Sci 2018; 59:45-53. [PMID: 29305606].

29. Douglas RM, Alam NM, Silver BD, McGill TJ, Tschetter WW, Prusky GT. Independent visual threshold measurements in the two eyes of freely moving rats and mice using a virtual-reality optokinetic system. Vis Neurosci 2005; 22:677-84. [PMID: 16332278].

30. Prusky GT, Alam NM, Beekman S, Douglas RM. Rapid quantification of adult and developing mouse spatial vision using a virtual optomotor system. Invest Ophthalmol Vis Sci 2004; 45:4611-6. [PMID: 15557474].

31. Wright CB, Chrenek MA, Feng W, Getz SE, Duncan T, Pardue MT, Feng Y, Redmond TM, Boatright JH, Nickerson JM. The Rpe65 rd12 allele exerts a semidominant negative effect on vision in mice. Invest Ophthalmol Vis Sci 2014; 55:2500-15. [PMID: 24644049].

32. Jiang Y, Qi X, Chrenek MA, Gardner C, Boatright JH, Grossniklaus HE, Nickerson JM. Functional principal component analysis reveals discriminating categories of retinal pigment epithelial morphology in mice. Invest Ophthalmol Vis Sci 2013; 54:7274-83. [PMID: 24114543].

33. Boatright JH, Dalal N, Chrenek MA, Gardner C, Ziesel A, Jiang Y, Grossniklaus HE, Nickerson JM. Methodologies for analysis of patterning in the mouse RPE sheet. Mol Vis 2015; 21:40-60. [PMID: 25593512].

34. Markand S, Baskin NL, Chakraborty R, Landis E, Wetzstein SA, Donaldson KJ, Priyadarshani P, Alderson SE, Sidhu CS, Boatright JH, Iuvone PM, Pardue MT, Nickerson JM. IRBP deficiency permits precocious ocular development and myopia. Mol Vis 2016; 22:1291-308. [PMID: 27829784].

35. Zivin JA, Bartko JJ. Statistics for disinterested scientists. Life Sci 1976; 18:15-26. [PMID: 1250059].

36. Yung M, Klufas MA, Sarraf D. Clinical applications of fundus autofluorescence in retinal disease. Int J Retina Vitreous 2016; 2:12-[PMID: 27847630].

37. Massengill MT, Ahmed CM, Lewin AS, Ildefonso CJ. Neuroinflammation in Retinitis Pigmentosa, Diabetic Retinopathy, and Age-Related Macular Degeneration: A Minireview. Adv Exp Med Biol 2018; 1074:185-91. [PMID: 29721943].

38. Silverman SM, Wong WT. Microglia in the Retina: Roles in Development, Maturity, and Disease. Annu Rev Vis Sci 2018; 4:45-77. [PMID: 29852094].

39. Shapiro L, Weis WI. Structure and biochemistry of cadherins and catenins. Cold Spring Harb Perspect Biol 2009; 1:a003053-[PMID: 20066110].

40. Yang X, Chung JY, Rai U, Esumi N. Cadherins in the retinal pigment epithelium (RPE) revisited: P-cadherin is the highly dominant cadherin expressed in human and mouse RPE in vivo. PLoS One 2018; 13:e0191279-[PMID: 29338041].

41. Saksens NT, Krebs MP, Schoenmaker-Koller FE, Hicks W, Yu M, Shi L, Rowe L, Collin GB, Charette JR, Letteboer

SJ, Neveling K, van Moorsel TW, Abu-Ltaif S, De Baere E, Walraedt S, Banfi S, Simonelli F, Cremers FP, Boon CJ, Roepman R, Leroy BP, Peachey NS, Hoyng CB, Nishina PM, den Hollander AI. Mutations in CTNNA1 cause butterfly-shaped pigment dystrophy and perturbed retinal pigment epithelium integrity. Nat Genet 2016; 48:144-51. [PMID: 26691986].

42. Donaldson KJ, Sellers JT, Boatright JH, Nickerson JM. Alpha-catenin is a novel marker for identifying abnormal morphology following surgical damage of the RPE. Invest Ophthalmol Vis Sci 2017; 58:624-.

43. Chrysostomou V, Galic S, van Wijngaarden P, Trounce IA, Steinberg GR, Crowston JG. Exercise reverses age-related vulnerability of the retina to injury by preventing complement-mediated synapse elimination via a BDNF-dependent pathway. Aging Cell 2016; [PMID: 27613664].

44. Chrysostomou V, Kezic JM, Trounce IA, Crowston JG. Exercise Protects Aged Retinal Ganglion Cells from Pressure-Induced Injury. ARVO Meeting Abstracts 2012; 53(6):4679.

45. Chrysostomou V, Kezic JM, Trounce IA, Crowston JG. Forced exercise protects the aged optic nerve against intraocular pressure injury. Neurobiol Aging 2014; 35:1722-5. [PMID: 24524967].

46. Kim DY, Jung SY, Kim CJ, Sung YH, Kim JD. Treadmill exercise ameliorates apoptotic cell death in the retinas of diabetic rats. Mol Med Rep 2013; 7:1745-50. [PMID: 23620139].

47. Ishiyama N, Sarpal R, Wood MN, Barrick SK, Nishikawa T, Hayashi H, Kobb AB, Flozak AS, Yemelyanov A, Fernandez-Gonzalez R, Yonemura S, Leckband DE, Gottardi CJ, Tepass U, Ikura M. Force-dependent allostery of the alpha-catenin actin-binding domain controls adherens junction dynamics and functions. Nat Commun 2018; 9:5121-[PMID: 30504777].

48. Kim SY, Yang HJ, Chang YS, Kim JW, Brooks M, Chew EY, Wong WT, Fariss RN, Rachel RA, Cogliati T, Qian H, Swaroop A. Deletion of aryl hydrocarbon receptor AHR in mice leads to subretinal accumulation of microglia and RPE atrophy. Invest Ophthalmol Vis Sci 2014; 55:6031-40. [PMID: 25159211].

49. Bubis E, Sher I, Skaat A, Sharvit-Ginon I, Szalapak AM, Moroz I, Kalter-Leibovici O, Rotenstreich Y. Blue Autofluorescence Fundus Imaging for Monitoring Retinal Degeneration in Royal College of Surgeons Rats. Transl Vis Sci Technol 2019; 8:26-[PMID: 30834174].

50. Sparrow JR, Duncker T. Fundus Autofluorescence and RPE Lipofuscin in Age-Related Macular Degeneration. J Clin Med 2014; 3:1302-21. [PMID: 25774313].

51. Sparrow JR, Wu Y, Nagasaki T, Yoon KD, Yamamoto K, Zhou J. Fundus autofluorescence and the bisretinoids of retina. Photochem Photobiol Sci 2010; 9:1480-9. [PMID: 20862444].

52. Zanzottera EC, Ach T, Huisingh C, Messinger JD, Freund KB, Curcio CA. Visualizing Retinal Pigment Epithelium Phenotypes in the Transition to Atrophy in Neovascular Age-Related Macular Degeneration. Retina 2016; 36:S26-39. [PMID: 28005661].

53. Zanzottera EC, Ach T, Huisingh C, Messinger JD, Spaide RF, Curcio CA. Visualizing Retinal Pigment Epithelium Phenotypes in the Transition to Geographic Atrophy in Age-Related Macular Degeneration. Retina 2016; 36:S12-25. [PMID: 28005660].

Articles are provided courtesy of Emory University and the Zhongshan Ophthalmic Center, Sun Yat-sen University, P.R. China. The print version of this article was created on 21 August 2019. This reflects all typographical corrections and errata to the article through that date. Details of any changes may be found in the online version of the article.